



Original Paper

Permeability Damage Mechanism and Evolution of Gas-Bearing Coal Seams Induced by Drilling Fluid

LingRui Kong,^{1,2} YongJiang Luo^{1,2,5}, JianXin Tang,^{1,2} YanLei Wang,³ Fang Yuan,^{1,2} Shuang Li,^{1,2} and YongJin Hao⁴

Received 21 December 2022; accepted 7 May 2023
Published online: 27 May 2023

Gas drainage is critical for underground coal mining in coal seams that contain high coalbed methane. We propose an underground pressurized drilling method to overcome the difficulty of drilling drainage hole along such coal seams, whereby water-based drilling fluid is used instead of pure water or air to clean the borehole. However, drilling fluid leakage can cause a serious reduction in coal seam permeability and correspondingly changing its gas production characteristics. Therefore, it is important to clarify the damage characteristic for estimating the gas production capacity of drainage hole along such coal seams. In this paper, the permeability damage characteristics of contaminated coal sample were studied using a core flow test method. Results confirmed that the permeability of the contaminated coal samples decreased significantly because of water-sensitive damage, water locking, and bentonite and polymer molecule plugging. In addition, the longer infiltration time and higher effective stress were harmful to permeability. Because higher gas pressure more likely opens the blocked pores and fractures, the permeability of the contaminated coal sample increased significantly with the improvement of inlet gas pressure. Meanwhile, the intrusion of water and solid phase into coal sample decreased the influence of stress on its permeability. This study has theoretical and practical significance in supporting the reformation of the underground pressurized drilling methods and drilling fluid design.

KEY WORDS: Coalbed methane, Drilling fluid, Overbalanced drilling, Permeability damage, Stress sensitivity.

INTRODUCTION

As a by-product gas in coal seams, coalbed methane (CBM) has emerged as an important unconventional natural gas (Taheri et al., 2017), which is also relevant to underground mining disasters such as gas explosions (Tong et al., 2018; Wang et al., 2020) and coal and gas outbursts (Wang et al., 2013; Du et al., 2020). CBM production from shallow minable coal seams has become prominent for resource utilization demands and mine safety (Karacan et al., 2011), and underground drainage with boreholes has become an enforcement measure for mines with high CBM.

¹State Key Laboratory of Coal Mine Disaster Dynamics and Control, Chongqing University, Chongqing 404100, China.

²School of Resources and Safety Engineering, Chongqing University, Chongqing 404100, China.

³Chongqing Bureau of Geology and Minerals Exploration, Chongqing 404100, China.

⁴China Coal Technology and Engineering Group Xian Research Institute, Xi'an 710077, Shaanxi, China.

⁵To whom correspondence should be addressed; e-mail: luoyj16@cqu.edu.cn

The borehole drainage of CBM is the most efficient method for underground mine gas prevention and control (Zhou et al., 2016). There are two types of extraction boreholes, namely crossing and bedding boreholes (Wang et al., 2014). Where drilling crossing boreholes must have a service gallery in the rock formation under the coal seam, it is a time-consuming and costly method (Liu et al., 2020). Compared to the crossing boreholes method, drainage CBM with bedding borehole has become the preferred method for coal seams that contain large amounts of CBM because of its advantage of time saving by eliminating the service gallery construction (Li et al., 2020b). At present, major underground drilling methods include water-based, air-based, and dry drilling methods with spiral drill pipes (Han et al., 2018; Li et al., 2020a). However, it is a challenge to use these methods in tectonically developed coal seams where abnormal in situ stress developed CBM accumulation (Tu et al., 2019; Cheng & Pan, 2020). Although drilling in complex formation is common in surface drilling projects and although several methods have been developed to overcome the adverse factors of drilling, it is difficult to use these methods directly because the majority of underground boreholes are horizontal or inverted holes. The formed borehole wall for these holes is in a free state and does not restrict the pore pressure and in situ geo-stress, leading to difficulties in overcoming borehole creep and collapse caused by the reserved CBM pressure and in situ geo-stress (Zhai et al., 2015; Zhao et al., 2020). Thus, coal production is typically delayed due to CBM extraction limitations (Zhou et al., 2016).

In this paper, we propose an underground pressurized drilling method to ensure the smooth drilling of boreholes in coal seams. As indicated in Figure 1, the drilling system consists of a slush pump, a pressurized slush tank, a borehole mouth-mounted sealing device, pressure-controlled solid-liquid separator, and underground drill rig. The drilling fluid is pressurized using a slush pump (to inhibit gas gushing into the borehole and to equalize the in situ formation stress), a borehole mouth-mounted sealing device, and a pressure-controlled solid-liquid separator during the drilling process.

Drilling fluid plays a key role in the drilling process. Based on different formation conditions, researchers have developed various drilling fluids that can inhibit wellbore instability and lost circulation effectively during oil and gas development, such as high-performance water-based drilling fluids,

which can maintain stability and inhibit shale dispersion at high temperatures (Akpan et al., 2019), drilling fluid with added boron nitride nanoparticles, which has good rheological properties in low temperature condition and is used in natural gas hydrate drilling (Maiti et al., 2021), and fuzzy ball drilling fluid, which is an environment-friendly drilling fluid used to control CBM wellbore collapse (Zheng et al., 2018a; Zhang et al., 2019). Compared to other types of drilling fluids, water-based drilling fluids are used diffusely in CBM drilling because their raw materials are inexpensive, environment-friendly, and safe. The fluid rheology, inhibition, and plugging performance of water-based drilling can be adjusted by adding additives such as polymers, surfactants, and sealing materials (Chen et al., 2019; Sun et al., 2020).

However, drilling fluid can cause serious reservoir damage (Ni et al., 2019). Previous studies on oil and gas drilling indicate that drilling fluid infiltration into a reservoir can cause particle aggregation and blockage, polymer gel blockage, water sensitivity damage, and water locking damage, which block the effective seepage channel and influence the migration of oil and gas (Zhao et al., 2019; Wang & Zhou, 2020; Seright & Brattekas, 2021). Compared to conventional oil and gas reservoirs, coal has characteristics of low original porosity, micropore development, low permeability, and strong adsorption capacity (Huang et al., 2022). Meanwhile, coal is a typical stress sensitive material whose permeability would significantly reduce with stress compression (Zheng et al., 2020). Researchers are committed to optimizing the drilling fluid formula to control lost circulation and reduce the damage rate (Kang et al., 2014; Freire Soares et al., 2018; Lyu et al., 2019). Several methods have been proposed to evaluate reservoir damage accurately (Okere et al., 2020; Liu et al., 2022). However, there has been only limited research on permeability damage mechanism and evolution characteristics of a coal seam, although this is extremely important for reducing coal seam damage.

Therefore, we attempted to investigate the permeability damage mechanism and evolution of coal seams induced by drilling fluid. First, the core flow test method was used to evaluate the extent of permeability damage. The extents of water sensitivity, water locking, and solid invasion damages were analyzed by scanning electron microscopy (SEM), nuclear magnetic resonance (NMR) spectroscopy, and other test methods. The effect of

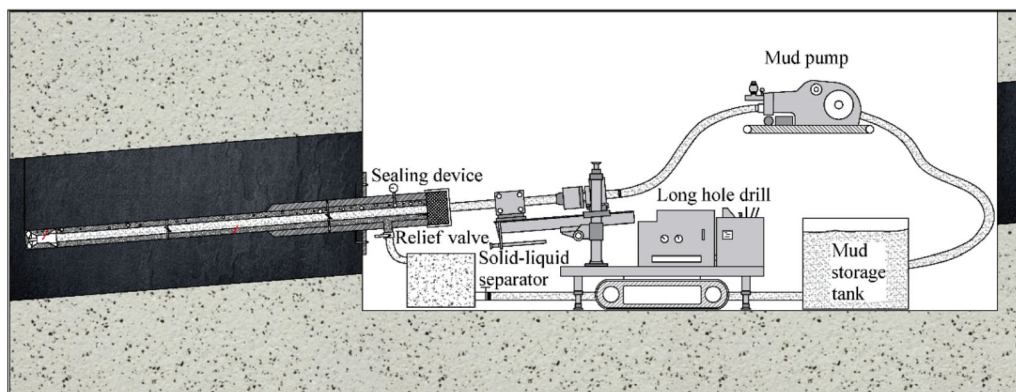


Figure 1. Sketch of pressurized drilling method.

infiltration time was also discussed. Finally, the time-dependent stress sensitivity of contaminated coal was studied and the effects of confining and gas pressures on contaminated coal were compared.

MATERIALS AND METHODS

Specimen Preparation

The coal samples used in this study were bituminous coal from Shenmu in Shaanxi Province. The coal samples were processed into cylinders each with diameter of 50 mm and height of 100 mm. The longitudinal wave velocity of each sample was tested using an ultrasonic detector to ensure the uniformity of the coal samples. Coal samples with similar P-wave characters were used. The pretreatment scheme is presented in Table 1 and Figure 2. Coal samples were divided into eight types. The natural coal samples were raw coal pillars without any pretreatment. The raw coal samples were dried at 378.15 K for 24 h to obtain dry coal samples. The pretreatment method of drilling fluid pollution and saturated water coal samples was as follows. The dried coal samples were soaked in the fluid to emulate the fluid filtration process with 2 MPa fluid pressure for predetermined times. The weights of the coal samples before and after pretreatment were recorded to calculate their moisture contents.

Water-based drilling fluids have several advantages including low cost and stability. Moreover, water supply to coal mines is usually available. Therefore, water-based drilling fluids are the preferred drilling medium in the pressurized drilling

method. We chose polymer additives, solid-phase materials as drilling mud material mixed with water to prepare the drilling fluids. The additive materials contained mainly 8 wt.% bentonite, 0.5 wt.% carboxymethyl cellulose (CMC), 0.1 wt.% potassium polyacrylate (K-PAM), and 0.5 wt.% sodium carbonate (Na_2CO_3) (Fig. 3). The performance of the drilling fluid was tested per the API test standards (Saleh, 2022). The density, apparent viscosity, and filter loss of the drilling fluids were 1.06 g/cm^3 , 26 mPa s, and 6.8 ml, respectively.

Experimental Methodology

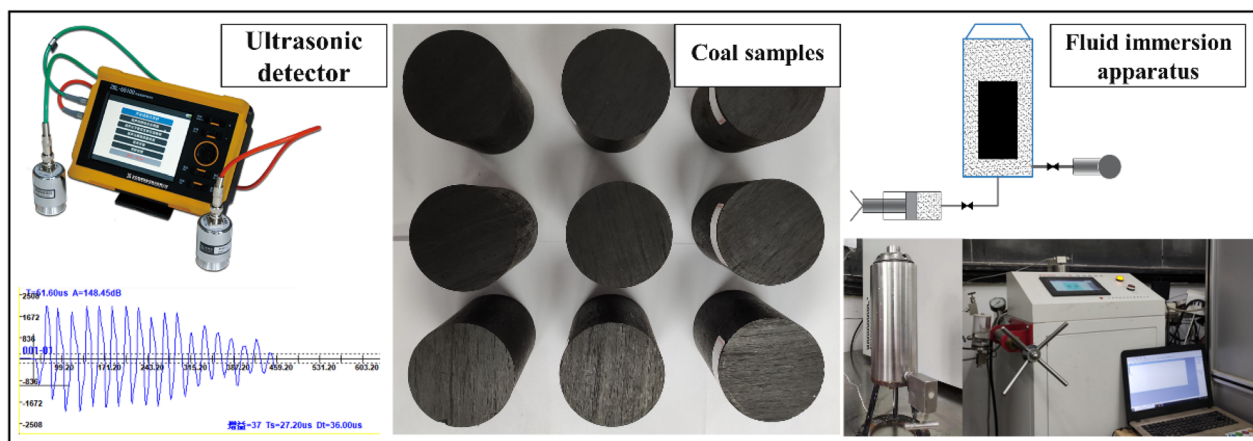
Coal Samples Analysis Experiments

The proximate analysis confirmed that the moisture content (M_{ad}) was 6.48%, ash content (A_{ad}) 7.60%, volatile content (V_{ad}) 33.47%, and fixed carbon content (FC_{ad}) 52.45%. X-ray diffraction (XRD) analysis using a D8 Advance X-ray diffractometer (Bruker Company, Germany) was performed to determine the mineral composition of the coal samples, and the results indicated that the main minerals of the coal were kaolinite (7%), chlorite (1%), illite (2%), quartz (6%), feldspar (2%), calcite (2%), and amorphous (80%).

Contact angle is a key parameter for evaluating the capillary pressure and relative permeability of porous sample, and the contact angle was tested by a JC-PHa contact angle meter. SEM was used to analyze the surface microstructure of the raw and contaminated coal samples. A low-field NMR Carr–Purcell–Meiboom–Gill pulse sequence was used to

Table 1. Coal sample preparation details

Sample	Pretreatment			Moisture content (%)
	Method	Pressure	Time	
CND	Dried by a vacuum dryer	–	–	0
CN0	Untreated	–	–	3.58
CN1	Immersion in drilling fluid	2 MPa	1 h	5.89
CN3			3 h	5.95
CN6			6 h	6.40
CN12			12 h	6.54
CN24			24 h	6.79
CNW	Immersion in water	2 MPa	24 h	6.51

**Figure 2.** Coal sample preparation.

measure the fluid relaxation process in the samples with an external magnetic field by a MacroMR12-150H-I NMR system (Suzhou Niumag Analytical Instrument Corporation), and the relaxation time (T_2) distribution spectrum was obtained as well. Given that a coal skeleton has no relaxation signal, the fluid relaxation characteristics of the saturated water coal samples could reflect their pore distribution (Liang et al., 2020). The pore distribution was calculated using Eqs. S1 – S3 (Supplementary Information). The water distribution of the coal samples at different drilling fluid pollution times was analyzed by NMR imaging.

Furthermore, using a briquetting machine, approximately 70 g of pulverized coal with particle sizes in the range of 60–80 mesh and water was mixed, forming coal briquettes with diameter of 50 mm and height of 25 mm. The resulting cylindrical coal briquettes were immersed in drilling fluid

after installing strain gauges, and the strain evolution within 24 h was recorded.

Gas Permeability Test Methodology

To assess the permeability damage characteristics of the drilling fluid in coal seams, a self-designed rock seepage device was used to test the changes in permeability (Fig. 4). Pretreated coal samples were placed in the core holder and high-pure nitrogen was injected from the inlet after confining pressure and axial pressure was applied. Under four different confining pressure conditions (ranging from 2 to 5 MPa), the permeability was tested with gas pressures ranging from 0.2 to 1.6 MPa. Gas flow was recorded at the outlet when it was stable. Permeability was calculated based on Darcy's law (Eq. S4, Supplementary Information).

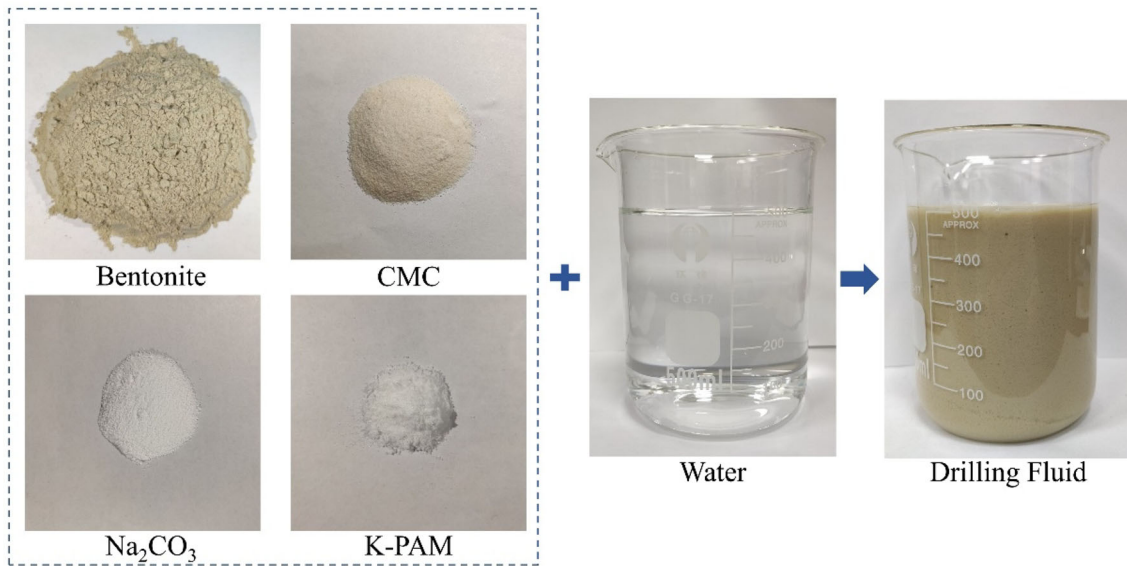


Figure 3. Drilling fluid.

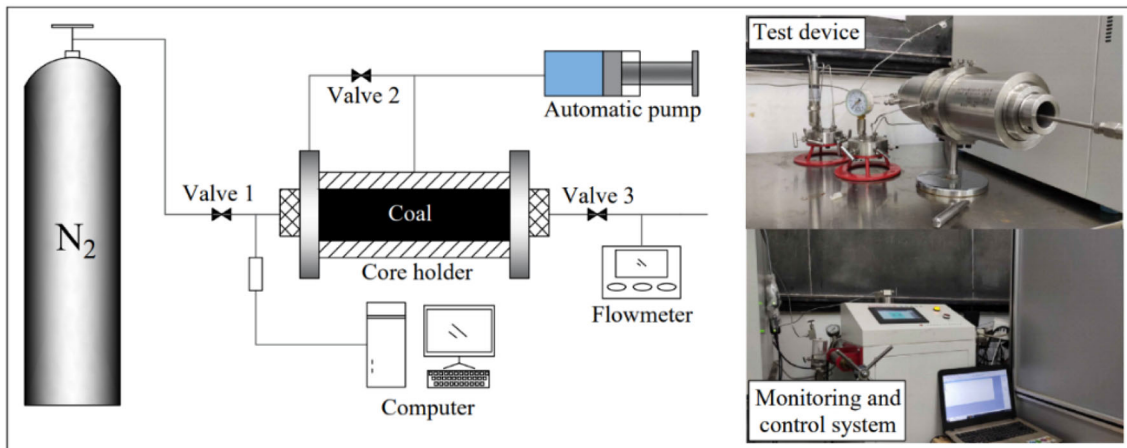


Figure 4. Gas permeability testing diagram.

RESULTS AND DISCUSSION

Figure 5 shows the permeability of coal samples with 3 MPa confining pressure. The gas permeability of four coal samples with the same gas pressure demonstrated the following trend: $CND > CN0 > CNW > CN24$. Among these, the gas permeability of samples CND and $CN0$ decreased initially with increase in pore pressure; it was directly proportional to pore pressure when it exceeded 1 MPa. Gas permeability of coal is related closely to the pro-

cesses of gas flow and gas adsorption. At the low pore pressure stage, the gas adsorption capacity of coal was enhanced with increase in gas pressure, which caused the adsorption expansion of the coal matrix and narrowing of the seepage channel. Moreover, the influence of the Klinkenberg effect on gas flow in the coal samples increased gradually with decrease in gas pressure (Zou et al., 2016; Bobo et al., 2019; Meng et al., 2021). Consequently, the gas permeability of the coal samples tended to decrease with increasing pore pressure. However, with

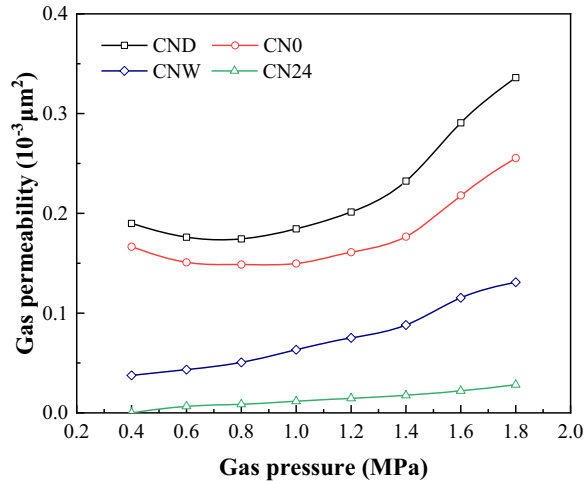


Figure 5. Gas permeability of coal samples.

increment of gas pressure, the gas adsorption capacity of the coal saturated gradually, and the influence of the Klinkenberg effect was weakened. Afterward, the decrease in effective stress and expansion of seepage space were the main reasons for the increase in permeability.

However, unlike samples CND and CN0, the gas permeabilities of samples CNW and CN24 increased as a function of pore pressure because the preferential adsorption of water reduced coal matrix swelling due to gas adsorption. Thus, the permeability of the coal samples was mainly influenced by the reduction in effective stress and by the expansion of seepage channel. To describe the permeability damage of the coal samples, D_k was defined as the permeability damage rate; it can be calculated using Eq. S5 (Supplementary Information).

Figure 6 displays the gas permeability and permeability damage rate of four coal samples at 1 MPa gas pressure, with the permeability of sample CND as the initial value. The permeability of the coal samples was correlated negatively with the confining pressure for the seepage space reduced with increasing of confining pressure. Compared with dry coal samples, the average permeability damage rate of coal samples CN0 and CNW increased by 20.55% and 71.79%, respectively. Correspondingly, the moisture contents of samples CN0 and CNW increased from 0% to 3.58% and 6.51% (Table 1), respectively, indicating that water saturation was a major contributor to the gas permeability of the coal samples. Two possible reasons for this damage are

water sensitivity and water locking damages (Li et al., 2022).

Water Sensitivity Damage of Coal

The proximate analysis indicated that ash content of the coal was 7.6%. Based on XRD analysis, clay minerals (kaolinite, chlorite, and illite) were found to account for 10% of coal samples. The clay minerals could experience hydration, expansion, and dispersion in water, thus increasing gas flow resistance, which would imply that the coal had a certain water sensitivity.

Figure 7 displays the volumetric strain of a briquette sample at different contamination times. The process of volumetric strain evolution can be divided into three stages. In the first stage ($t < 1$ h), when the drilling fluid was injected into the beaker, the volumetric strain of the briquette sample was negative due to the irregular deformation caused by the difference in infiltration rate. In the second stage ($1 \text{ h} < t < 5$ h), the volumetric strain of the briquette sample increased rapidly due to water swelling of the coal matrix and clay minerals when the drilling fluid infiltrated the briquette sample rapidly. Then, as mud cake was formed and a water-saturated state was reached gradually, the evolution process of volumetric strain entered the third stage ($t > 5$ h), in which the volumetric strain increased slowly and was stabilized gradually. The evolution process of the volumetric strain with drilling fluid infiltration time was similar to that of the moisture content of the coal samples. Water swelling of the coal matrix and clay minerals, which was related to water saturation, caused the narrowing and blockage of pores and fissures, thus reducing the effective seepage channel of the coal samples. These microstructure evolutions led to the decline of gas permeability.

Water Locking Damage of Coal

Water locking damage occurs because when water is adsorbed by coal, a concave surface is formed at the gas/water interface in the pore throat, generating additional capillary pressure in the coal as water saturation increases. Capillary resistance is inversely proportional to pore radius and contact angle and it is directly proportional to surface tension (Eq. S6, Supplementary Information). Measur-

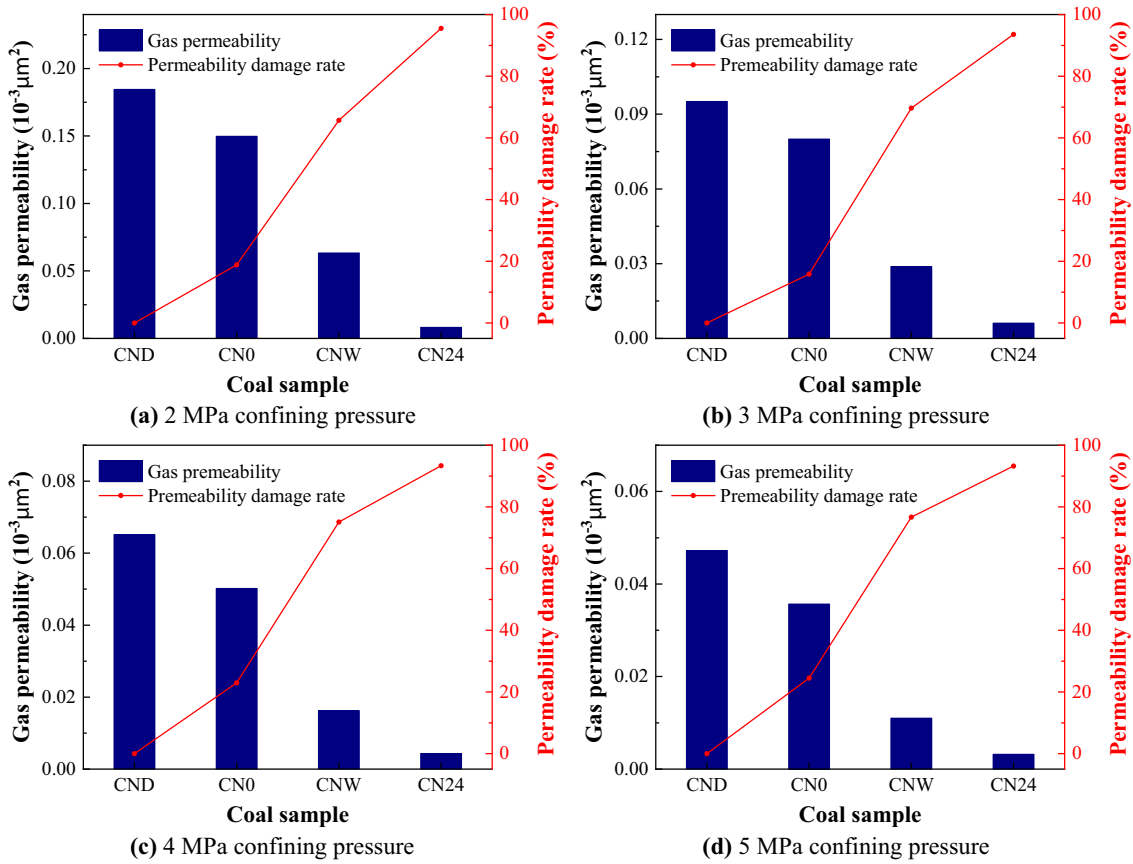


Figure 6. Permeability damage rate of coal samples with different confining pressures.

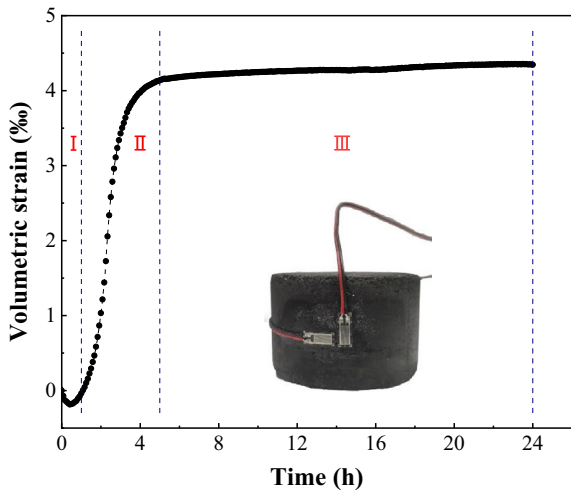


Figure 7. Volumetric strain change with contamination time in drilling fluid.

ing the pore distribution and contact angle of the coal samples can reflect the capillary pressure.

As a prominent nondestructive testing method, NMR is used widely for analyzing coal microstructure (Zheng et al., 2018b; Zhang et al., 2022). Based on Eq. S3 (Supplementary Information), pore size was correlated positively with T_2 , and the T_2 distribution can reflect the pore characteristics of coal samples. Figure 8a displays the T_2 spectrum of the coal samples. Only one evident peak was observed in the T_2 spectrum. The T_2 value peak was between 0.5 and 0.7 ms, indicating that the coal micropores were more developed (Yao et al., 2010; Yao & Liu, 2012). To quantify the pore distribution of the coal samples, their pore size distributions were calculated based on Eq. S3 (Supplementary Information), where $\rho = 5.4 \text{ nm/ms}$, $F_s = 2$, and the conversion coefficient $C = 10.8 \text{ nm/ms}$ (Xie et al., 2015). The porosity of the coal samples was obtained by cor-

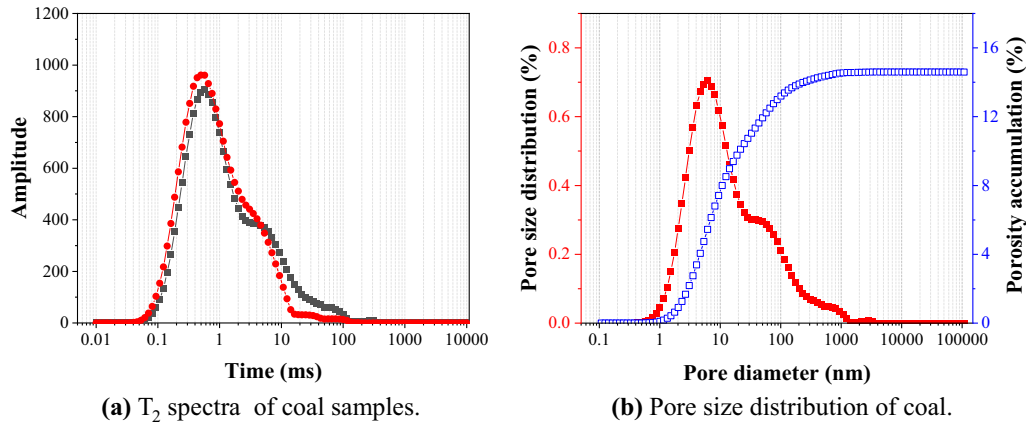


Figure 8. NMR test results of coal samples.

recting the value of T_2 . The results are presented in Figure 8b.

Based on pore diameter (d) and the coal pore classification method proposed by Hodot (1966), the coal pores can be classified into micropores ($d \leq 10$ nm), transitional pores ($10 \text{ nm} < d \leq 100$ nm), mesopores ($100 \text{ nm} < d \leq 1000$ nm), and macropores pores ($d > 1000$ nm). As indicated in Figure 8b, the porosity of the coal was 14.59% and the proportions of porosity in the four pore ranges were as follows: micropores (50.85%) > transitional pores (38.15%) > mesopores (10.54%) > macropores pores (0.46%). The NMR results indicated that the coal pores were predominantly micropores and transitional pores. Moreover, the average contact angle between the coal rock and water was 51.62° (Fig. 9), and the wettability was water-wetting (Li et al., 2022). Therefore, the water lock effect could substantially reduce the permeability of the coal samples.

Figure 10 displays the evolution of gas flow rate with gas pressure under 2 MPa confining pressure, and the gas flow rate was found to be correlated positively with gas pressure. With increasing gas pressure, the evolution curves changed gradually from a nonlinear concave curve to a linear curve. No clear gas flow was observed in sample CN24 when gas pressure was less than 0.6 MPa, indicating that flow channel blockage was related to critical gas pressure. Correspondingly, with increasing gas pressure, additional blocked flow channels were reopened.

Based on the evolution characteristics of the gas flow rate, the gas breakthrough pressure (P_b) is de-

finied as the intersection point of the linearly extending evolution curve at the high gas pressure and abscissa axis (Xu et al., 2019). Gas breakthrough pressure is the critical pressure when the gas can overcome the internal resistance of the coal and form a continuous flow. This is a key parameter that reflects coal microstructure, which correlates with the stress state of the coal and developing degree, shape, and connectivity of the pores and fissures (Wu et al., 2020). Figure 10 displays the gas breakthrough pressures of the coal samples, which were in the following order: CND (1.077 MPa) < CN0 (1.094 MPa) < CNW (1.145 MPa) < CN24 (1.248 MPa). The connectivity of the pores and fissures in the coal samples decreased and the gas flow resistance increased due to the aggravation of water locking damage and water sensitivity damage with moisture content, leading to the increase in gas breakthrough pressure. In addition, the microflow channels in the coal samples were blocked by bentonite particles and polymer molecules, and the flow channel inlet was blocked by mud cake, leading to further increase in gas breakthrough pressure.

Solid Invasion Damage of Coal

As indicated in Table 1, the moisture content of sample CN24 was close to that of sample CNW. However, the average permeability damage rate of sample CN24 was 93.46%, which was greater than that of sample CNW. This was because the bentonite particles in the drilling fluid were deposited on the coal surface and invaded into the coal samples dur-

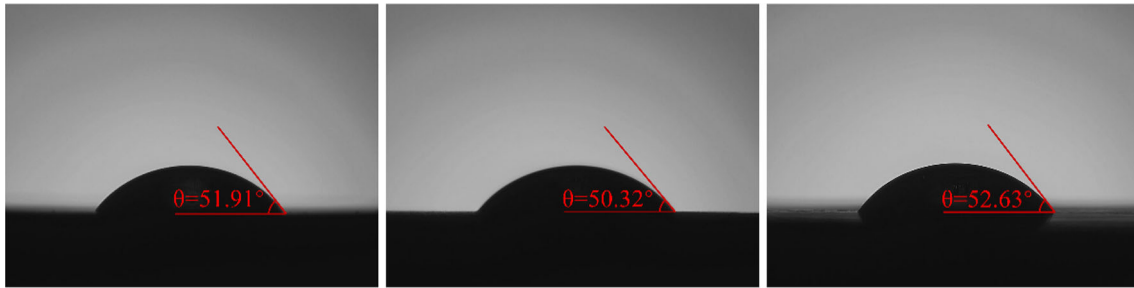


Figure 9. Contact angle of coal.

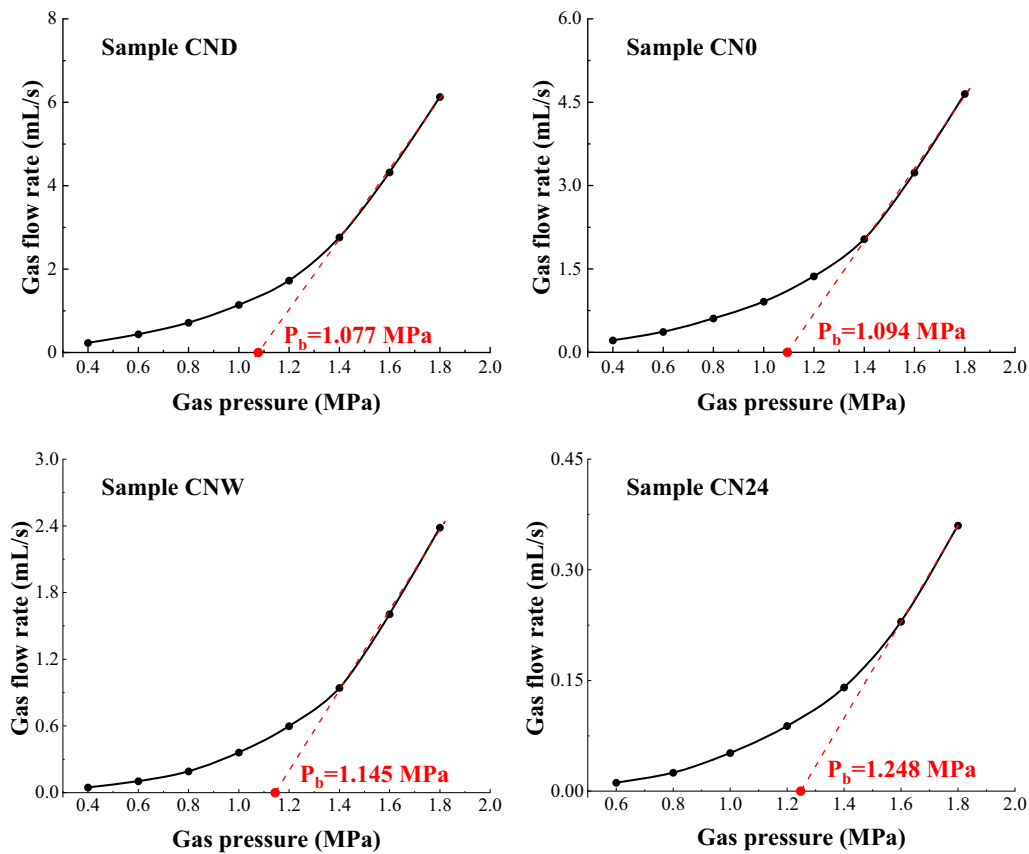
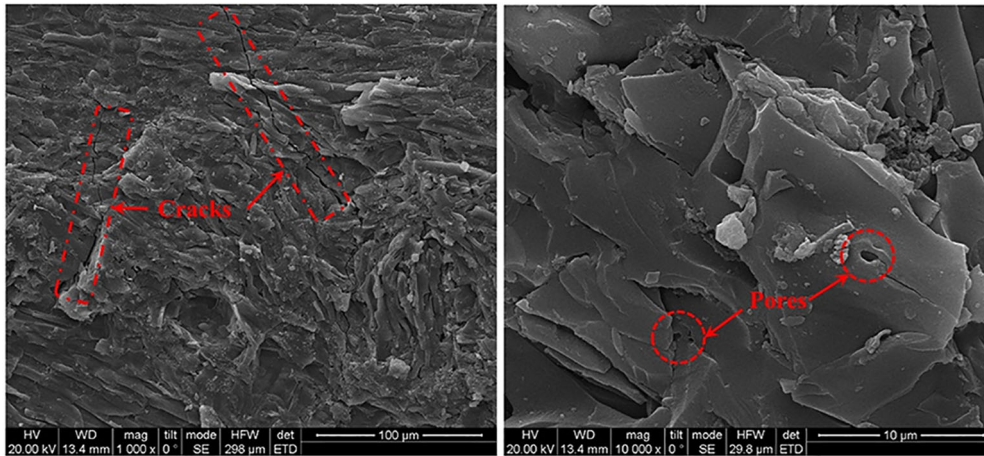


Figure 10. Gas flow rate and gas breakthrough pressures of coal samples.

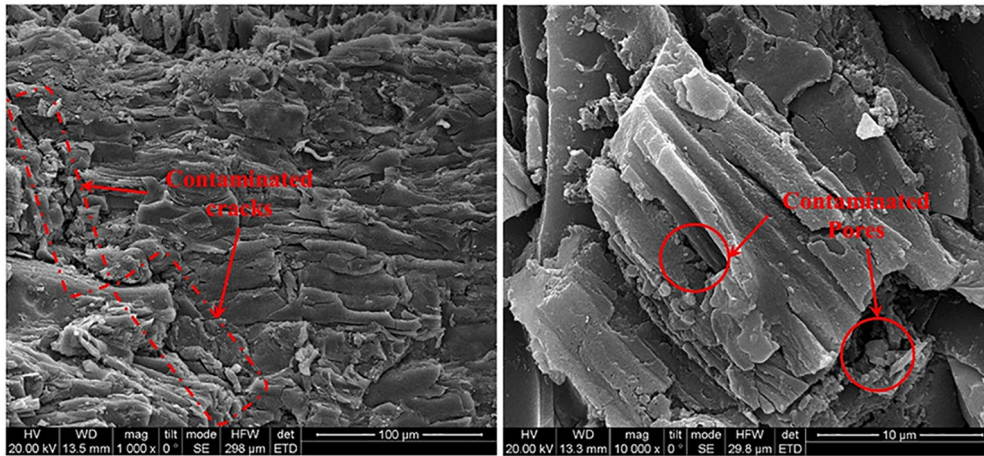
ing the filtration process, which blocked part of the pores and fissures. Although the plugging of the seepage channel reduced the leakage of drilling fluid, it caused a decline in the coal sample permeability (Al Jaber et al., 2021).

Figure 11 displays SEM images of the raw and contaminated coal samples. After immersion of the coal samples in drilling fluid, the microflow channels

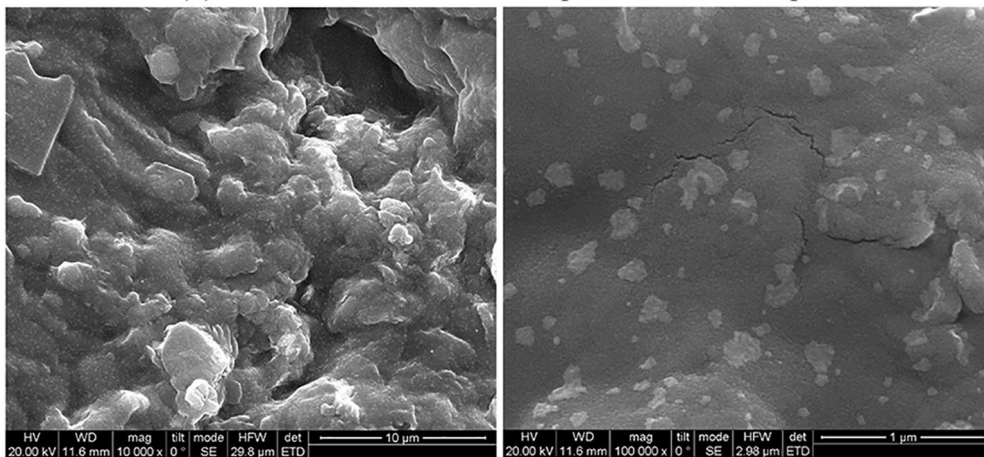
in the coal samples were blocked by bentonite and polymer molecules, and filter cake blocked the flow channel inlet, leading to further permeability decline (Lei et al., 2017). As indicated in Figure 6, the permeability damage rate of sample CN24 increased by 21.67% relative to sample CNW. However, this only accounted for 23.19% of the total permeability damage of sample CN24. This result confirmed that



(a) Original cracks and pores of coal sample



(b) Contaminated cracks and pores of coal sample



(c) Residual filter cake on contaminated coal sample

Figure 11. SEM images of coal samples.

water sensitivity and water locking damages were the main reason of coal permeability decrease.

Effect of Infiltration Time

During drilling, the permeability damage of the contaminated coal seam could be aggravated with the extension of drilling fluid infiltration time. The process of drilling fluid infiltration into a coal seam under a drilling fluid pressure of 2 MPa within 24 h was emulated in a laboratory, and the permeability of the coal samples was tested. Based on Eq. S5 (Supplementary Information), the permeability damage rate was calculated with the permeability of coal sample CN0 as the initial value.

As indicated in Figure 12, the gas permeabilities of the coal samples under 1 MPa gas pressure and 3 MPa confining pressure were taken as examples. The permeability damage of the coal samples was most significant in the first 6 h. Compared with the gas permeability of sample CN0, that of sample CN6 reduced to $0.012 \times 10^{-3} \mu\text{m}^2$, corresponding to a relative decrease in 85%. When the infiltration drilling fluid time was 24 h, the gas permeability decreased from $0.08 \times 10^{-3} \mu\text{m}^2$ to $0.006 \times 10^{-3} \mu\text{m}^2$, and the permeability damage rate was 92.5%. Correspondingly, the gas permeability of sample CN24 decreased by $0.0057 \times 10^{-3} \mu\text{m}^2$ and the permeability damage rate increased by 7.14% compared with that of sample CN6. This result indicated that the gas permeability of the contaminated coal samples decreased gradually with the extension of drilling fluid infiltration time. When the drilling fluid infiltration time was between 3 and 6 h, the gas permeability and permeability damage rate curves had an evident inflection point. Subsequently, the permeability stabilized gradually with time.

The permeability damage rates of the contaminated coal samples decreased with increase in gas pressure because the seepage channel plugging could be relieved with increasing gas pressure. As the gas pressure increased from 0.6 to 1.6 MPa, the change in permeability damage rate of coal sample CN1 decreased from 81.51% to 40.97%, whereas that of sample CN24 merely decreased from 95.17% to 86.76%. These results indicated that the damage degree of the coal samples was aggravated with increased soaking time in the drilling fluid. Consequently, it was more difficult to improve the pore connectivity, and the permeability of coal samples changed marginally with the gas pressure.

The infiltration of the drilling fluid filtrate and blockage of the seepage channels by polymer and bentonite particles were the reasons for the coal permeability damage. As shown in Figure 13, the water distribution in the coal samples was obtained using magnetic resonance imaging (MRI). Within the red circle, the blue area represents an anhydrous coal matrix, whereas the other area's color gradually changes from blue to red with increase in moisture content. The blue area decreased and the dark areas with irregular bands expanded as contamination time increased, indicating that the mud filtrate diffused gradually in the coal samples and occupied the seepage space, which could reduce the gas permeability of the coal sample. Therefore, we should reduce drilling time as much as possible during pressurized drilling of gas drainage boreholes in gas-bearing coal seams. Effective measures of leakage prevention should be taken to reduce the pollution range of the drilling fluid. After pressurized drilling, the long-term contaminated section of the borehole was the main scope of implementing permeability improvement technology.

Stress Sensitivity of Contaminated Coal

The distribution characteristics of pores and fractures in coal determine its permeability. Moreover, the microstructure of coal is extremely sensitive to stress. However, the infiltration of drilling fluid could influence the microstructure of coal and then influence its stress sensitivity. Therefore, the evolution characteristics of stress sensitivity of contaminated coal were studied. C_p was defined as the stress sensitivity coefficient to describe the change rate of permeability with increasing stress (Eq. S7, Supplementary Information).

As indicated in Figure 14, the permeability of the coal samples decreased with increase in confining pressure. The stress sensitivity coefficient (C_p) under low confining pressure was greater than that under high confining pressure. This is because the original pores and fractures in the coal samples could be regarded as weak interlayers, which could be the first to deform and reduce the seepage channels with increasing confining pressure (Kumar et al., 2018). Under low confining pressure, the anti-deformation ability of the original pores and fractures was low, whereas the compressibility of the fractures was strong. However, with increase in confining pressure, the influence of compaction

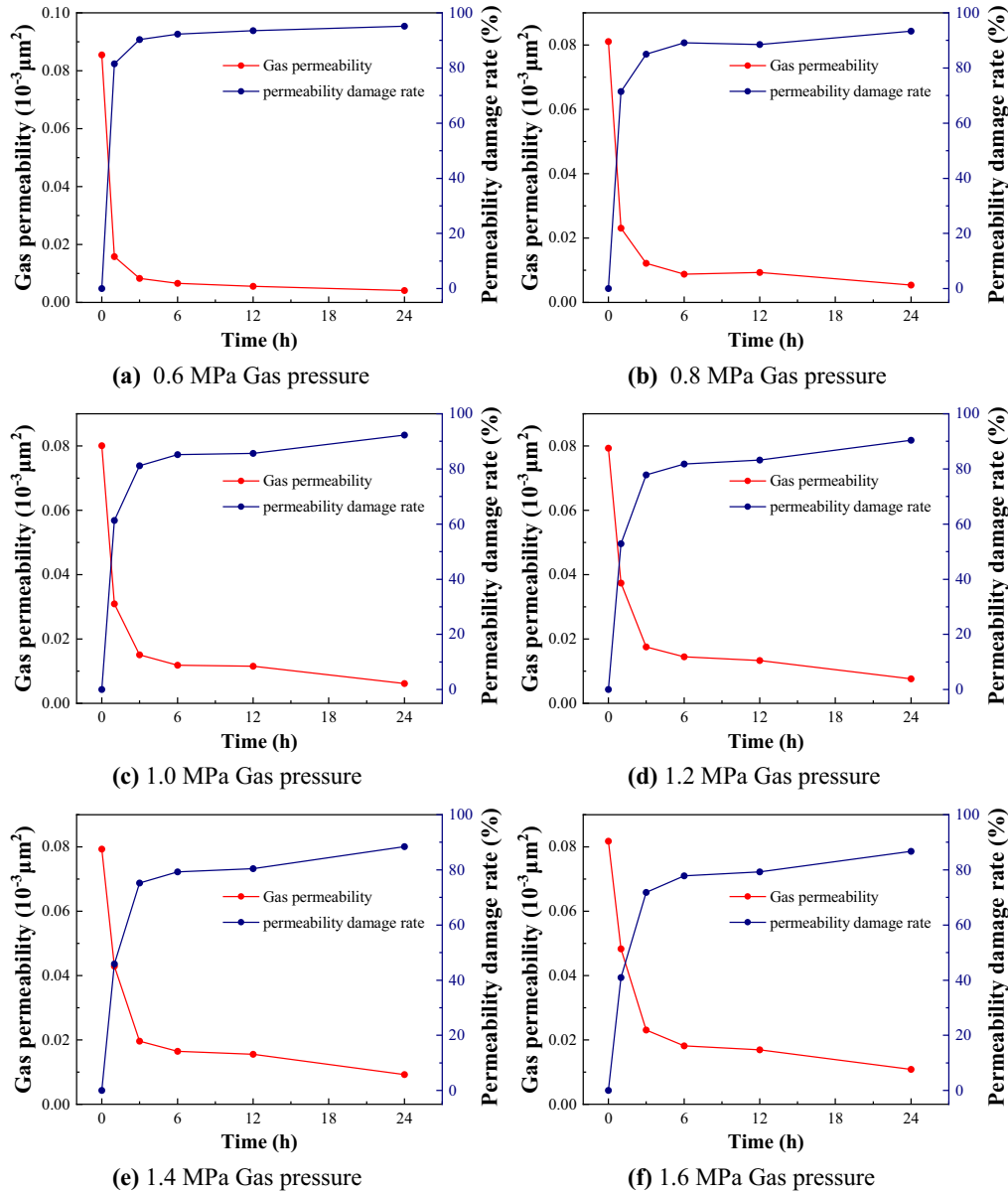


Figure 12. Permeability damage rate based on considerations of time.

forced the mineral particles and coal matrix to contact gradually, thus improving the anti-deformation ability of the fractures. Therefore, the gas permeability as well as the stress sensitivity of coal samples decreased with increase in confining pressure.

Table 2 presents the average stress sensitivity coefficient of the coal samples when the confining pressure increased from 2 to 5 MPa. Overall, the stress sensitivity coefficient of the contaminated coal

samples decreased with infiltration time, indicating that the compressibility of fractures was weakened. C_f was defined as cleat compressibility, and its relationship with permeability and confining pressure is (Wu et al., 2021):

$$k = k_0 e^{(-3C_f(\sigma - \sigma_0))}, \tag{1}$$

where k is gas permeability (10⁻³ μm²), k_0 is initial permeability (10⁻³ μm²), C_f is cleat compressibility, σ

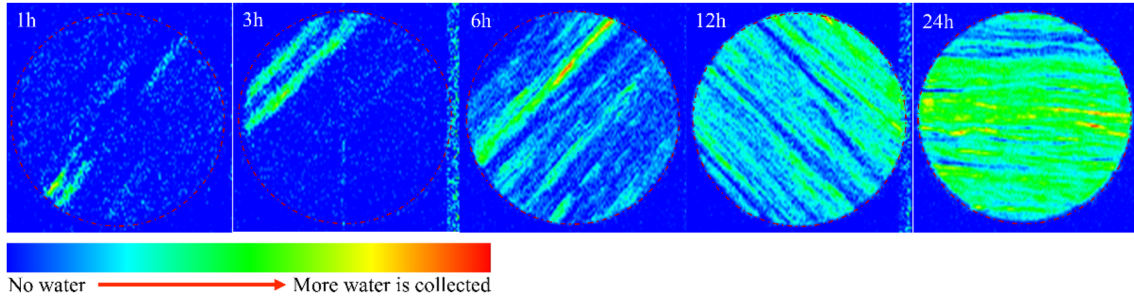


Figure 13. MRI of water distribution in coal samples.

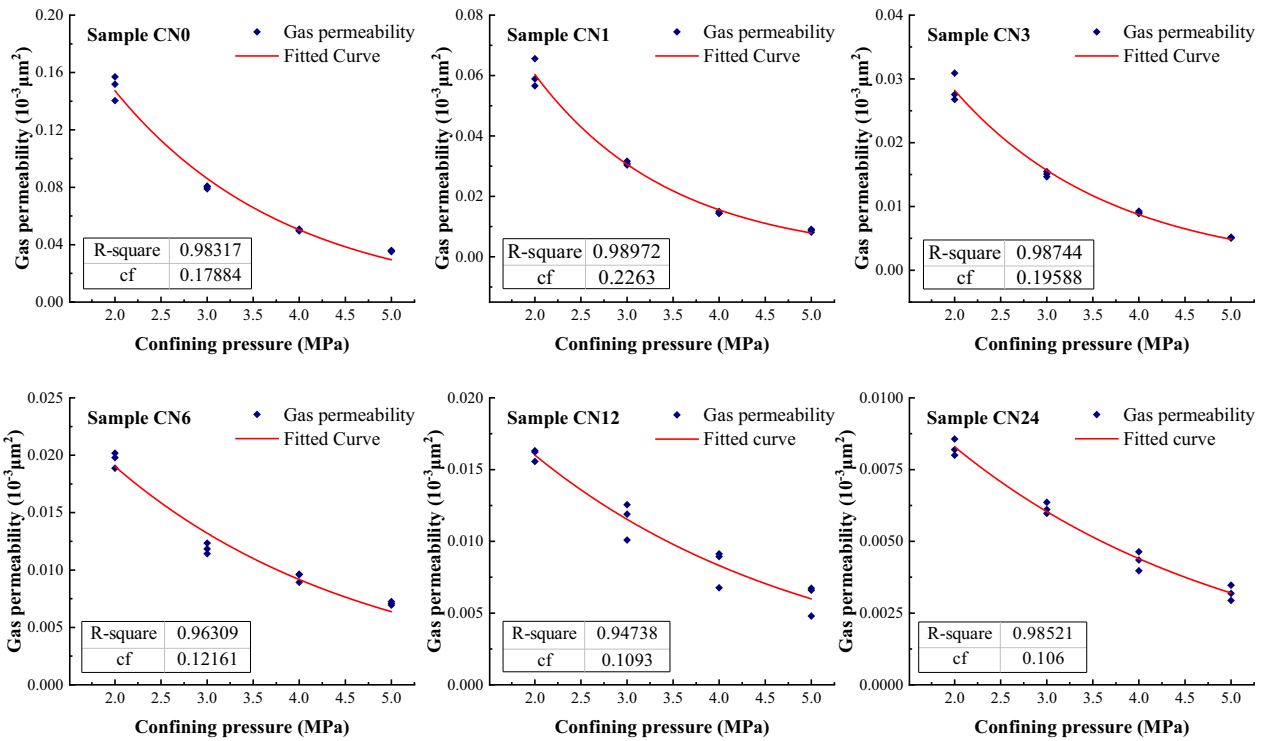


Figure 14. Gas permeability variation with confining pressure.

Table 2. Permeability damage with confining pressure and fitting results

Sample	C_p	C_f	k_0	σ_0	R^2
CN0	0.254	0.179	0.147	2	0.98317
CN1	0.285	0.226	0.060	2	0.98972
CN3	0.274	0.196	0.028	2	0.98744
CN6	0.213	0.122	0.019	2	0.96309
CN12	0.207	0.109	0.016	2	0.94738
CN24	0.204	0.106	0.008	2	0.98306

is confining pressure (MPa), and σ_0 is initial confining pressure (MPa).

Equation 1 was used to fit the permeability evolution curve with the confining pressure. The fitting results are displayed in Figure 14 and Table 2. The permeability damage rate and C_f of sample CN0 were smaller than those of samples CN1 and CN3 because hydration reduced the deformation resistance of the coal samples. However, with increasing drilling fluid infiltration time, the C_f of the contaminated coal samples decreased, indicating that the

compressibility of the fractures decreased. Two possible reasons can explain this phenomenon. Firstly, the coal sample creep and compaction caused by drilling fluid pressure could have improved the deformation resistance of the fractures with time. Secondly, the pores and fractures of the coal samples were filled with drilling fluid filtrate. Moreover, the drilling fluid filtrate took much work to compress. Nevertheless, it could provide resistance to pore and fracture deformation under increasing confining pressure. Correspondingly, the permeability damage rate of the coal samples caused by the increase in confining pressure decreased with drilling fluid infiltration time.

The permeability of the coal samples changed with the infiltration of drilling fluid and was influenced by the gas and confining pressures (Zhang et al., 2021). Therefore, effective stress was used to represent the comprehensive influence of the gas and confining pressures, thus:

$$\sigma_e = \sigma_c - \frac{1}{2}(P_1 + P_2), \quad (2)$$

where σ_e is effective stress (MPa), σ_c is confining pressure (MPa), and P_1 and P_2 are gas pressure (MPa) at inlet and outlet, respectively.

Figure 15 displays the evolution curve of gas permeability with effective stress. In the first stage, the confining pressure was fixed, and the gas pressure increased, corresponding to a decrease in effective stress. With increasing gas pressure, additional blocked flow channels were reopened. Correspondingly, the permeability of the contaminated coal samples increased with decreasing effective stress. The permeability of sample CN0 decreased with decreasing effective stress at low gas pressures due to the combination of gas adsorption and the Klinkenberg effect. In the second stage, the gas pressure was fixed and the confining pressure was increased. The permeability of the coal samples decreased with increasing effective stress because the original pores and fractures in the coal samples could be compressed and seepage channels reduced with increasing confining pressure. Compared with confining pressure, coal permeability was more sensitive to changes in effective stress induced by gas pressure because the increased confining pressure only influenced the fracture opening. Conversely, the increased gas pressure not only expanded the pores and fractures but also alleviated the blockage of the seepage channels (Xu et al., 2019).

Arguably, gas pressure influenced the connectivity of the pores and fractures more likely than confining pressure, especially for coal samples with long drilling fluid infiltration time. The reduction of gas pressure could cause a significant decline in gas drainage efficiency in contaminated coal seams during gas drainage. Therefore, anti-seepage measures should be taken to reduce the drilling fluid pollution degree and scope during drilling. It is necessary to employ pressure-releasing technology and take permeability enhancement measures after drilling, which could reduce effective stress, promote gas desorption, and improve the coal seam permeability.

CONCLUSIONS

In this study, we evaluated the infiltration of drilling fluid that caused permeability damage for gas-bearing coal seams. The coal seam damage mechanism was analyzed. The influence of effective stress and pollution time on the coal permeability evolution was investigated. This study provides a theoretical basis for the coal seam protection design of the underground pressurized drilling methods. Based on the research undertaken, the following conclusions can be drawn.

1. The permeability of coal samples was closely related to moisture content because the gas flow channel was narrowed and blocked by water-sensitive and water lock damages. Bentonite and polymer molecules occupied the gas flow channel, which decreased in the pore connectivity and permeability of the coal samples.
2. The permeability damage increased as a function of drilling fluid infiltration time. Moreover, the permeability damage mainly occurred in the first 6 h of pollution and then it tended to stabilize.
3. The permeability of the coal samples was correlated negatively with the confining pressure. However, the influence of the confining pressure weakened with the extension of infiltration time because of the reduction of the fracture compressibility.
4. The permeability of the coal samples decreased with increase in effective stress. Based on the evolution of permeability with effective stress, gas pressure was more favorable in ameliorating the permeability of the contaminated coal sample.

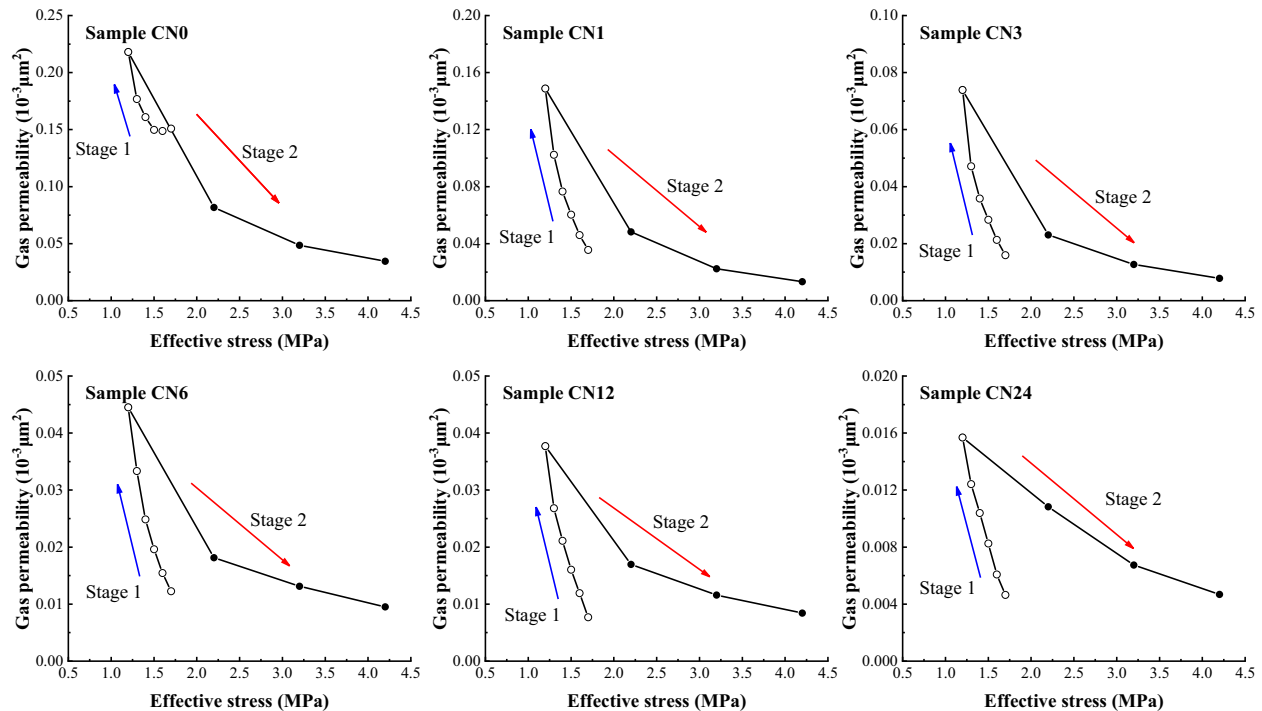


Figure 15. Gas permeability variation with effective stress..

ACKNOWLEDGMENTS

This work is financially supported by the State key laboratory of coal mine disaster dynamics and control Key Research Program (Grant No. 2011DA105287-zd202009), the Natural Science Foundation of Chongqing (Grant No. cstc2019jcyj-msxmX0633 & No. cstc2020jcyj-msxmX0972), which are gratefully acknowledged. The authors also thank to the editor and anonymous reviewers for their valuable advices.

DATA AVAILABILITY

All data generated or analyzed during this study are included in this published article.

DECLARATIONS

Conflict of Interest The authors declare that they have no known competing financial interests or personal relationships that could have appeared to influence the work reported in this paper.

SUPPLEMENTARY INFORMATION

The online version contains supplementary material available at <https://doi.org/10.1007/s11053-023-10212-5>.

REFERENCES

- Akpan, E. U., Enyi, G. C., Nasr, G., Yahaya, A. A., Ahmadu, A. A., & Saidu, B. (2019). Water-based drilling fluids for high-temperature applications and water-sensitive and dispersible shale formations. *Journal of Petroleum Science and Engineering*, *175*, 1028–1038.
- Al Jaber, J., Bageri, B. S., Adebayo, A. R., Patil, S., Barri, A., & Salin, R. B. (2021). Evaluation of formation damages during filter cake deposition and removal process: The effect of primary damage on secondary damage. *Petroleum Science*, *18*(4), 1153–1162.
- Bobo, L., Kang, Y., Peng, X., Jiang, X., Mei, Y., & Min, Z. (2019). An experimental study on permeability characteristics of coal with slippage and temperature effects. *Journal of Petroleum Science and Engineering*, *175*, 294–302.
- Chen, S., Shi, Y., Yang, X., Xie, K., & Cai, J. (2019). Design and evaluation of a surfactant-mixed metal hydroxide-based drilling fluid for maintaining wellbore stability in coal measure strata. *Energies*, *12*(10), 1862.
- Cheng, Y. P., & Pan, Z. J. (2020). Reservoir properties of Chinese tectonic coal: A review. *Fuel*, *260*, 116350.

- Du, F., Wang, K., Zhang, X., Xin, C., Shu, L., & Wang, G. (2020). Experimental study of coal-gas outburst: Insights from coal-rock structure, gas pressure and adsorptivity. *Natural Resources Research*, 29(4), 2481–2493.
- Freire Soares, A. S., Costa Marques, M. R., Caçada, L. A., Borges Filho, M. N., de Oliveira, L., & Petkowicz, C. (2018). Interaction of blockers on drilling fluids rheology and its effects on sealing of fractures and prevention of filtrate invasion. *Journal of Petroleum Science and Engineering*, 171, 260–270.
- Han, X. M., Zhang, Q. Q., Wang, S. F., Li, J. L., & Chen, D. T. (2018). Influence of polycrystalline diamond compact bit geometric parameters on drilling performance during gas drainage borehole in soft coal seam. *Advances in Mechanical Engineering*, 10(1), 9.
- Hodot, B. B. (1966). *Coal and Gas Outburst (Chinese Translation)*. China Coal Industry Press.
- Huang, Q., Wu, B., Liu, Y., Guo, Z., Wang, G., & Sun, L. (2022). Experimental and simulation investigations of the impact of polyacrylamide on CBM ad-/desorption. *Journal of Petroleum Science and Engineering*, 208, 109300.
- Kang, Y., Xu, C., You, L., Yu, H., & Zhang, D. (2014). Temporary sealing technology to control formation damage induced by drill-in fluid loss in fractured tight gas reservoir. *Journal of Natural Gas Science and Engineering*, 20, 67–73.
- Karacan, C. Ö., Ruiz, F. A., Cotè, M., & Phipps, S. (2011). Coal mine methane: A review of capture and utilization practices with benefits to mining safety and to greenhouse gas reduction. *International Journal of Coal Geology*, 86(2–3), 121–156.
- Kumar, H., Mishra, M. K., & Mishra, S. (2018). Laboratory investigation of gas permeability and its impact on CBM potential. *Journal of Petroleum Exploration and Production Technology*, 8(4), 1183–1197.
- Lei, M., Huang, W., Li, N., Jia, J., Li, J., Wang, Y., & Li, J. (2017). The damage mechanism of oil-based drilling fluid for tight sandstone gas reservoir and its optimization. *Journal of Petroleum Science and Engineering*, 158, 616–625. <https://doi.org/10.1016/j.petrol.2017.09.003>.
- Li, H., Ma, J. K., Wang, Z. Q., Wang, W., & Liu, Y. (2020a). A gas outburst prevention and control strategy for single thick coal seams with high outburst risk: A case study of Hudi Coal Mine in Qinshui Basin. *Energy Science & Engineering*, 8(7), 2471–2491.
- Li, H., Wang, W., Liu, Y. W., Ma, J. K., & Gao, H. (2020b). An integrated drilling, protection and sealing technology for improving the gas drainage effect in soft coal seams. *Energy Reports*, 6, 2030–2043.
- Li, Y. Z., Jiang, G. C., Li, X. Q., & Yang, L. L. (2022). Quantitative investigation of water sensitivity and water locking damages on a low-permeability reservoir using the core flooding experiment and NMR test. *ACS Omega*, 7(5), 4444–4456.
- Liang, Y. P., Tan, Y. T., Wang, F. K., Luo, Y., & Zhao, Z. (2020). Improving permeability of coal seams by freeze-fracturing method: The characterization of pore structure changes under low-field NMR. *Energy Reports*, 6, 550–561.
- Liu, H., Su, G., Okere, C. J., Li, G., Wang, X., Cai, Y., Wu, T., & Zheng, L. (2022). Working fluid-induced formation damage evaluation for commingled production of multi-layer natural gas reservoirs with flow rate method. *Energy*, 239, 122107.
- Liu, J., Yang, T., Wang, L., & Chen, X. (2020). Research progress in coal and gas co-mining modes in China. *Energy Science & Engineering*, 8(9), 3365–3376.
- Lyu, S. F., Wang, S. W., Chen, X. J., Shah, S. M., Li, R., Xiao, Y., Dong, Q., & Gu, Y. (2019). Experimental study of a degradable polymer drilling fluid system for coalbed methane well. *Journal of Petroleum Science and Engineering*, 178, 678–690.
- Maiti, M., Bhaumik, A. K., & Mandal, A. (2021). Performance of water-based drilling fluids for deepwater and hydrate reservoirs: Designing and modelling studies. *Petroleum Science*, 18(6), 1709–1728.
- Meng, Y., Li, Z. P., & Lai, F. P. (2021). Influence of effective stress on gas slippage effect of different rank coals. *Fuel*, 285, 119207.
- Ni, X. M., Liu, Z. D., & Wei, J. P. (2019). Quantitative evaluation of the impacts of drilling mud on the damage degree to the permeability of fractures at different scales in coal reservoirs. *Fuel*, 236, 382–393.
- Okere, C. J., Su, G., Zheng, L., Cai, Y., Li, Z., & Liu, H. (2020). Experimental, algorithmic, and theoretical analyses for selecting an optimal laboratory method to evaluate working fluid damage in coal bed methane reservoirs. *Fuel*, 282, 118513.
- Saleh, T. A. (2022). Experimental and analytical methods for testing inhibitors and fluids in water-based drilling environments. *TRAC Trends in Analytical Chemistry*, 149, 116543.
- Seright, R., & Brattekas, B. (2021). Water shutoff and conformance improvement: An introduction. *Petroleum Science*, 18(2), 450–478.
- Sun, P., Han, M., Cao, H., Liu, W., Zhang, S., & Zhu, J. (2020). Development and performance evaluation of solid-free drilling fluid for CBM reservoir drilling in central Hunan. *Energies*, 13(18), 4857.
- Taheri, A., Sereshki, F., Ardejani, F. D., & Mirzaghobanali, A. (2017). Simulation of macerals effects on methane emission during gas drainage in coal mines. *Fuel*, 210, 659–665.
- Tong, X., Fang, W. P., Yuan, S. Q., Ma, J., & Bai, Y. (2018). Application of Bayesian approach to the assessment of mine gas explosion. *Journal of Loss Prevention in the Process Industries*, 54, 238–245.
- Tu, Q. Y., Cheng, Y. P., Ren, T., Wang, Z., Lin, J., & Lei, Y. (2019). Role of tectonic coal in coal and gas outburst behavior during coal mining. *Rock Mechanics and Rock Engineering*, 52(11), 4619–4635.
- Wang, H. F., Cheng, Y. P., Wang, W., & Xu, R. (2014). Research on comprehensive CBM extraction technology and its applications in China's coal mines. *Journal of Natural Gas Science and Engineering*, 20, 200–207.
- Wang, H., Gu, S., & Chen, T. (2020). Experimental investigation of the impact of CO, C₂H₆, and H₂ on the explosion characteristics of CH₄. *ACS Omega*, 5(38), 24684–24692.
- Wang, J., & Zhou, F. J. (2020). Cause analysis and solutions of water blocking damage in cracked/non-cracked tight sandstone gas reservoirs. *Petroleum Science*, 18(1), 219–233.
- Wang, L., Cheng, Y. P., Ge, C. G., Chen, J.-X., Li, W., Zhou, H.-X., & Hai-feng, W. (2013). Safety technologies for the excavation of coal and gas outburst-prone coal seams in deep shafts. *International Journal of Rock Mechanics and Mining Sciences*, 57, 24–33.
- Wu, T., Pan, Z. J., Connell, L. D., Liu, B., Fu, X., & Xue, Z. (2020). Gas breakthrough pressure of tight rocks: A review of experimental methods and data. *Journal of Natural Gas Science and Engineering*, 81, 103408.
- Wu, Y., Tao, S., Tian, W., Chen, H., & Chen, S. (2021). Advantageous seepage channel in coal seam and its effects on the distribution of high-yield areas in the Fanzhuang CBM Block, Southern Qinshui Basin. *China. Natural Resources Research*, 30(3), 2361–2376.
- Xie, S. B., Yao, Y. B., Chen, J. Y., & Yao, W. (2015). Research of micro-pore structure in coal reservoir using low-field NMR. *Journal of China Coal Society*, 40, 170–176.
- Xu, L., Zhu, F. H., Zha, F. S., Chu, C. F., & Yang, C. (2019). Effects of gas pressure and confining pressure on gas flow behavior in saturated cohesive soils with low permeability. *Engineering Geology*, 260, 105241.

- Yao, Y. B., & Liu, D. M. (2012). Comparison of low-field NMR and mercury intrusion porosimetry in characterizing pore size distributions of coals. *Fuel*, *95*, 152–158.
- Yao, Y., Liu, D., Che, Y., Tang, D., Tang, S., & Huang, W. (2010). Petrophysical characterization of coals by low-field nuclear magnetic resonance (NMR). *Fuel*, *89*(7), 1371–1380.
- Zhai, C., Xu, Y. M., Xiang, X. W., Yu, X., Zou, Q., & Zhong, C. (2015). A novel active prevention technology for borehole instability under the influence of mining activities. *Journal of Natural Gas Science and Engineering*, *27*, 1585–1596.
- Zhang, L., Huang, M., Xue, J., Li, M., & Li, J. (2021). Repetitive mining stress and pore pressure effects on permeability and pore pressure sensitivity of bituminous coal. *Natural Resources Research*, *30*(6), 4457–4476.
- Zhang, S., Wu, C., Fang, X., Liu, N., Jiang, X., & Han, J. (2022). Mapping of stress sensitivity affected by water variation to microscopic pore distributions in medium- and high-rank coals. *Natural Resources Research*, *31*(3), 1601–1619.
- Zhang, Y., Su, G., Zheng, L., Liu, D., Guo, Z., & Wei, P. (2019). The environmental friendliness of fuzzy-ball drilling fluids during their entire life-cycles for fragile ecosystems in coal-bed methane well plants. *Journal of Hazardous Materials*, *364*, 396–405.
- Zhao, H. B., Li, J. Y., Liu, Y. H., Wang, Y., Wang, T., & Cheng, H. (2020). Experimental and measured research on three-dimensional deformation law of gas drainage borehole in coal seam. *International Journal of Mining Science and Technology*, *30*(3), 397–403.
- Zhao, X., Qiu, Z. S., Sun, B. J., Liu, S. J., Xing, X., & Wang, M. (2019). Formation damage mechanisms associated with drilling and completion fluids for deepwater reservoirs. *Journal of Petroleum Science and Engineering*, *173*, 112–121.
- Zheng, L., Su, G., Li, Z., Peng, R., Wang, L., Wei, P., & Han, S. (2018a). The wellbore instability control mechanism of fuzzy ball drilling fluids for coal bed methane wells via bonding formation. *Journal of Natural Gas Science and Engineering*, *56*, 107–120.
- Zheng, S. J., Liu, Y., Pan, Y., Liu, T., & Du, D. (2020). The invasion of drilling fluid into coal under fluctuating wellbore pressure. *Arabian Journal of Geosciences*, *13*(9), 334.
- Zheng, S. J., Yao, Y. B., Liu, D. M., Cai, Y. D., & Liu, Y. (2018b). Characterizations of full-scale pore size distribution, porosity and permeability of coals: A novel methodology by nuclear magnetic resonance and fractal analysis theory. *International Journal of Coal Geology*, *196*, 148–158.
- Zhou, F. B., Xia, T. Q., Wang, X. X., Zhang, Y., Sun, Y., & Liu, J. (2016). Recent developments in coal mine methane extraction and utilization in China: A review. *Journal of Natural Gas Science and Engineering*, *31*, 437–458.
- Zou, J. P., Chen, W. Z., Yang, D. S., Yu, H. D., & Yuan, J. Q. (2016). The impact of effective stress and gas slippage on coal permeability under cyclic loading. *Journal of Natural Gas Science and Engineering*, *31*, 236–248.

Springer Nature or its licensor (e.g. a society or other partner) holds exclusive rights to this article under a publishing agreement with the author(s) or other rightsholder(s); author self-archiving of the accepted manuscript version of this article is solely governed by the terms of such publishing agreement and applicable law.